



Ethylene/ethane separation in a stable hydrogen-bonded organic framework through a gating mechanism

Yisi Yang^{1,4}, Libo Li^{2,4}, Rui-Biao Lin^{3,4}, Yingxiang Ye^{1,3}, Zizhu Yao¹, Ling Yang², Fahui Xiang¹, Shimin Chen¹, Zhangjing Zhang¹✉, Shengchang Xiang¹✉ and Banglin Chen³✉

Porous materials are very promising for the development of cost- and energy-efficient separation processes, such as for the purification of ethylene from ethylene/ethane mixture—an important but currently challenging industrial process. Here we report a microporous hydrogen-bonded organic framework that takes up ethylene with very good selectivity over ethane through a gating mechanism. The material consists of tetracyano-bicarbazole building blocks held together through intermolecular CN...H-C hydrogen bonding interactions, and forms as a threefold-interpenetrated framework with pores of suitable size for the selective capture of ethylene. The hydrogen-bonded organic framework exhibits a gating mechanism in which the threshold pressure required for guest uptake varies with the temperature. Ethylene/ethane separation is validated by breakthrough experiments with high purity of ethylene (99.1%) at 333 K. Hydrogen-bonded organic frameworks are usually not robust, yet this material was stable under harsh conditions, including exposure to strong acidity, basicity and a variety of highly polar solvents.

Separations are critical processes in chemical industry^{1,2}. The processes to separate and purify industrial commodities, such as distillation for gases and water, account for 10–15% of the global energy consumption¹. The development of alternative and energy-efficient separation technologies is therefore highly in demand^{3,4}. Physical adsorption in porous adsorbents that enable separation through pressure swing adsorption (PSA) and thermal swing adsorption⁴ is very promising in terms of energy saving. In fact, some adsorbents have already been implemented in industrial separations, for example, the titanosilicate molecular sieve ETS-4 for the industrial-scale separation of natural gas^{4,5}.

However, challenges and huge energy consumptions exist for the major industrial gas separations. For example, separating ethylene from ethane requires cryogenic distillation, a very energy-intensive but important step involving repeated distillation–compression cycling, which consumes up to about 800 PJ per year⁶, more than 0.3% of annual global energy consumption¹. In a common process for ethylene production, which is based on the cracking of heavier hydrocarbon fractions, followed by dehydrogenation reactions, the conversion yield of the latter step is only around 50 to 60%. Other processes such as catalytic dehydrogenation also give an equimolar mixture of C₂H₄ and C₂H₆. The upgrading of ethylene from the C₂H₄/C₂H₆ mixture through the energy-efficient adsorption separation would thus reap enormous global benefits.

Porous metal–organic frameworks (MOFs)^{7–15}, covalent organic frameworks (COFs)^{16,17} and hydrogen bonded-organic frameworks (HOFs)^{18,19} have been explored for gas separation and purification^{20–22}. The fact that MOFs are so well-suited to rational pore tuning and straightforward pore functionalization has led to good performances as adsorbents for several gas separations^{23–28}, but only a few examples of MOFs with very high selectivity have been realized, particularly for the hydrocarbon separations^{29–31}. Most

hydrocarbon separations are particularly challenging as they involve molecules with similar dimensions. For example, the dimensions of ethylene are about 3.28 × 4.18 × 4.84 Å³, whereas those of ethane are about 3.81 × 4.08 × 4.82 Å³ (refs. 32,33).

Furthermore, even for porous MOFs that seem to lend themselves well to high sieving separations from a structural point of view (considering their pore structures and window sizes), it is still very challenging to fulfil high separation performance due to their flexible nature: the pores are typically gradually enlarged under slightly higher pressures and therefore they also entrap the larger hydrocarbon, leading to co-adsorption. This effect was observed in the UTSA-200 MOF we recently developed for the removal of propyne (C₃H₄) from a mixture with propylene (C₃H₆)³⁴, which substantially diminished the separation performance and the purity of the separated product. We also reported very good sieving performance for UTSA-280 for ethylene/ethane separation²⁹. We attributed the high sieving separation to the rigidity of UTSA-280 constrained by the squarate linkers, which almost completely prevented ethane molecules from entering its pores. Given that most organic linkers within MOFs will undergo—at least to some extent—rotation and distortion under different stimulus such as temperatures and pressures^{35–37}, it has remained difficult to prepare rigid MOFs for high sieving separations of hydrocarbons.

Gate pressure adsorption phenomena are well established in porous materials³⁸. In general, adsorption/desorption is an equilibrium physical and exothermic process (Fig. 1), which means that increasing the adsorption temperature will favour the equilibrium to the left (less gas uptake), whereas increasing the gas pressure (concentration of gas) will favour the equilibrium to the right (more gas uptake) (Fig. 1). This means that the flexibility of porous materials is not necessarily a hindrance when it comes to the selective uptake of guests—we can make use of mechanisms such as gating phenomena

¹Fujian Provincial Key Laboratory of Polymer Materials, College of Chemistry and Materials Science, Fujian Normal University, Fuzhou, China. ²College of Chemistry and Chemical Engineering, Shanxi Key Laboratory of Gas Energy Efficient and Clean Utilization, Taiyuan University of Technology, Taiyuan, China. ³Department of Chemistry, University of Texas at San Antonio, One UTSA Circle, San Antonio, TX, United States. ⁴These authors contributed equally: Yisi Yang, Libo Li, Rui-Biao Lin. ✉e-mail: zzhang@fjnu.edu.cn; scxiang@fjnu.edu.cn; banglin.chen@utsa.edu

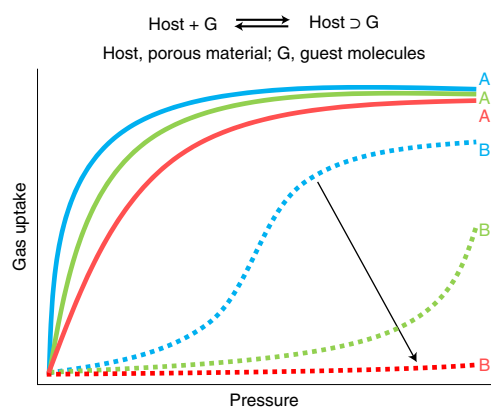


Fig. 1 | Tuning gate-pressures mechanism for highly selective gas separation. An illustration of the representative variations observed in typical gas adsorption isotherms of a flexible-robust adsorbent for smaller gas A and larger gas B at three different temperatures. The sorption equilibrium between the host (porous material) and the guest (G) is shown above. Blue, low temperature; green, medium temperature; red, high temperature; solid lines, smaller gas (A); dotted lines, larger gas (B). The black arrow indicates that the gate-opening pressure for the larger gas B gradually increases as the temperature increases. Although A is adsorbed at all temperatures, uptake of B is only at lower temperatures and its threshold pressure increases (uptake decreases) with increasing temperature. This means that the selectivity of the separation of an A/B mixture can be tuned by the conditions (temperature, pressure).

by which the opening of pores to fulfil gas separations depend on guest pressures and sometimes also temperatures (Fig. 1). The feature of adsorbate-dependent structural flexibility in a flexible $\text{Ca}(\text{H}_2\text{tcpb})$ MOF has been harnessed for temperature-dependent sieving separation of linear alkanes from the branched isomers—with molecular sizes of a large difference¹⁵. The open pore space in flexible MOFs with permanent porosity (so-called flexible-robust MOFs³⁹) enables them to take up smaller gas components before transforming into large-pore phases for the larger gases at relatively high pressures. This is different from fully flexible MOFs, in which the condensed phases show no gas adsorption under low pressures (closed pores), and then exhibit structural transformations to open phases (open pores) under gate-opening pressures, typically leading to significant co-adsorption of the counterpart gases. If such a material exhibits permanent small pores, it should be able to take up a large amount of the smaller hydrocarbon (guest A in Fig. 1), yet the co-adsorption of the larger hydrocarbon molecules (guest B) through the various temperatures, at correspondingly different gate pressures, can be controlled to minimize uptake of the larger molecules. The flexible-robust characteristic is the prerequisite to realize such unique tunable separation.

Compared with MOFs and COFs, HOFs are assembled by organic molecular building blocks through weak hydrogen bonding; HOF materials can thus be easily purified through simple recrystallization, showing great solution processability, recyclability and healing capability. This type of organic material can be straightforwardly processed into different forms such as spheres and membranes for the column and membrane gas separations, respectively.

Here we report a microporous HOF with tunable, temperature-dependent gate pressures for the separation of ethylene from ethane at 333 K. The framework, termed HOF-FJU-1, is a microporous hydrogen-bonded organic framework self-assembled from the simple organic molecule 3,3',6,6'-tetracyano-9,9'-bicarbazole (3). The recovered ethylene can reach the purity of 99.1% at 333 K, as established by the experimental breakthrough curve.

Results and discussion

The tetracyano-bicarbazole organic building block (3) was obtained from the cyanolization of 3,3',6,6'-tetrabromo-9,9'-bicarbazole (2) through the oxidative coupling reaction of 3,6-dibromocarbazole (Fig. 2a), which was confirmed by infrared, ¹H NMR, ¹³C NMR, elemental analysis and thermogravimetric analysis (TGA). The high-quality single crystals were recrystallized from a hot *N,N'*-dimethylformamide (DMF)-saturated solution of HOF-FJU-1 powders. Single-crystal X-ray diffraction studies showed that HOF-FJU-1 crystallizes in orthorhombic space group *Pnn2* (Supplementary Fig. 1 and Supplementary Table 1). In this HOF, there are three crystallographically unique bicarbazole molecules in its asymmetric units. Each bicarbazole unit is linked to four adjacent bicarbazoles by four pairs of CN...H-C hydrogen bonds with distances of 3.431–3.536 Å along the *ac* plane to form a single dia network (Fig. 2b,c, and Supplementary Figs. 2 and 6).

The void space in a single network allows the final structure to exhibit a threefold-interpenetrated array, showing distinct offset π - π interactions along the *a* axis with distances of 3.799–4.794 Å that may further enhance the rigidity of this type of flexible porous materials (Supplementary Figs. 3 and 4). Following triple interpenetration, there are still one-dimensional pore channels running along the crystallographic [100] direction with a void pore volume by ~20% of the total crystal cell, in which the large cages ($3.4 \times 6.2 \times 10.6 \text{ \AA}^3$) and the small necks ($3.4 \times 3.8 \times 5.3 \text{ \AA}^3$) are alternating (cages I and II in Supplementary Fig. 5). The pore window size of the channels is about $3.4 \times 5.3 \text{ \AA}^2$, calculated from projection of pore channels by taking account the van der Waals radius of atoms (Fig. 2d and Supplementary Fig. 5). The pore windows fit well to the molecular size of ethylene (Fig. 2e), which promotes our further investigation on potential sieving separation.

The thermal stability of HOF-FJU-1 was investigated by TGA and variable-temperature powder X-ray diffraction (PXRD) in an N_2 atmosphere (Supplementary Figs. 7 and 8). This HOF retained its framework following heating above 523 K. Notably, after vacuum outgassing of the as-synthesized sample at 423 K for 12 h, the crystal structure of guest-free HOF-FJU-1a was directly obtained on the basis of X-ray diffraction analysis in a single-crystal to single-crystal transformation manner, indicating the robustness of HOF-FJU-1 during desolvation. The framework with weak intermolecular interactions and pore structures are well preserved after guest removal, with only slight changes in parameters of crystal unit-cell (Supplementary Table 1). The minimum dimensions of window size in HOF-FJU-1a (3.4 – 3.8 \AA) match well with the minimum molecular dimension of C_2H_4 (3.28 \AA) over C_2H_6 (3.81 \AA). Accordingly, the relatively robust pore space with appropriate size rendered this HOF a potential adsorbent with a substantial sieving effect for ethylene/ethane separation.

Sorption of N_2 was performed at 77 K to verify the porosity of HOF-FJU-1a (Supplementary Fig. 9). Analysis of N_2 adsorption isotherms gives an experimental Brunauer–Emmett–Teller (Langmuir) surface area of 385 (431) $\text{m}^2 \text{ g}^{-1}$ (Supplementary Fig. 10, and Supplementary Tables 7 and 8). The pore size distribution of HOF-FJU-1a has been analysed based on Hovath–Kawazoe model, showing peaks centred at 6.0 and 11.4 \AA . For comparison, another pore size distribution has also been calculated using the Poreblazer program⁴⁰, indicating two types of pore cavities of 6.2 and 10.8 \AA , in line with the sorption results and crystallographic structure dimensions (Supplementary Figs. 5 and 11). According to IUPAC classification⁴¹, HOF-FJU-1a is a microporous material with pore size below 20 \AA . The amount of adsorbed N_2 in the first step is $75 \text{ cm}^3 \text{ g}^{-1}$ at $P/P_0 = 0.001$, corresponding to a pore volume of $\sim 0.12 \text{ cm}^3 \text{ g}^{-1}$. The total N_2 uptake at 77 K and 1 bar is $100 \text{ cm}^3 \text{ g}^{-1}$, which corresponds to a total pore volume of $\sim 0.15 \text{ cm}^3 \text{ g}^{-1}$, consistent with the theoretical value calculated from crystal structure ($0.17 \text{ cm}^3 \text{ g}^{-1}$). Similar stepwise adsorption isotherm was also observed for CO_2 in

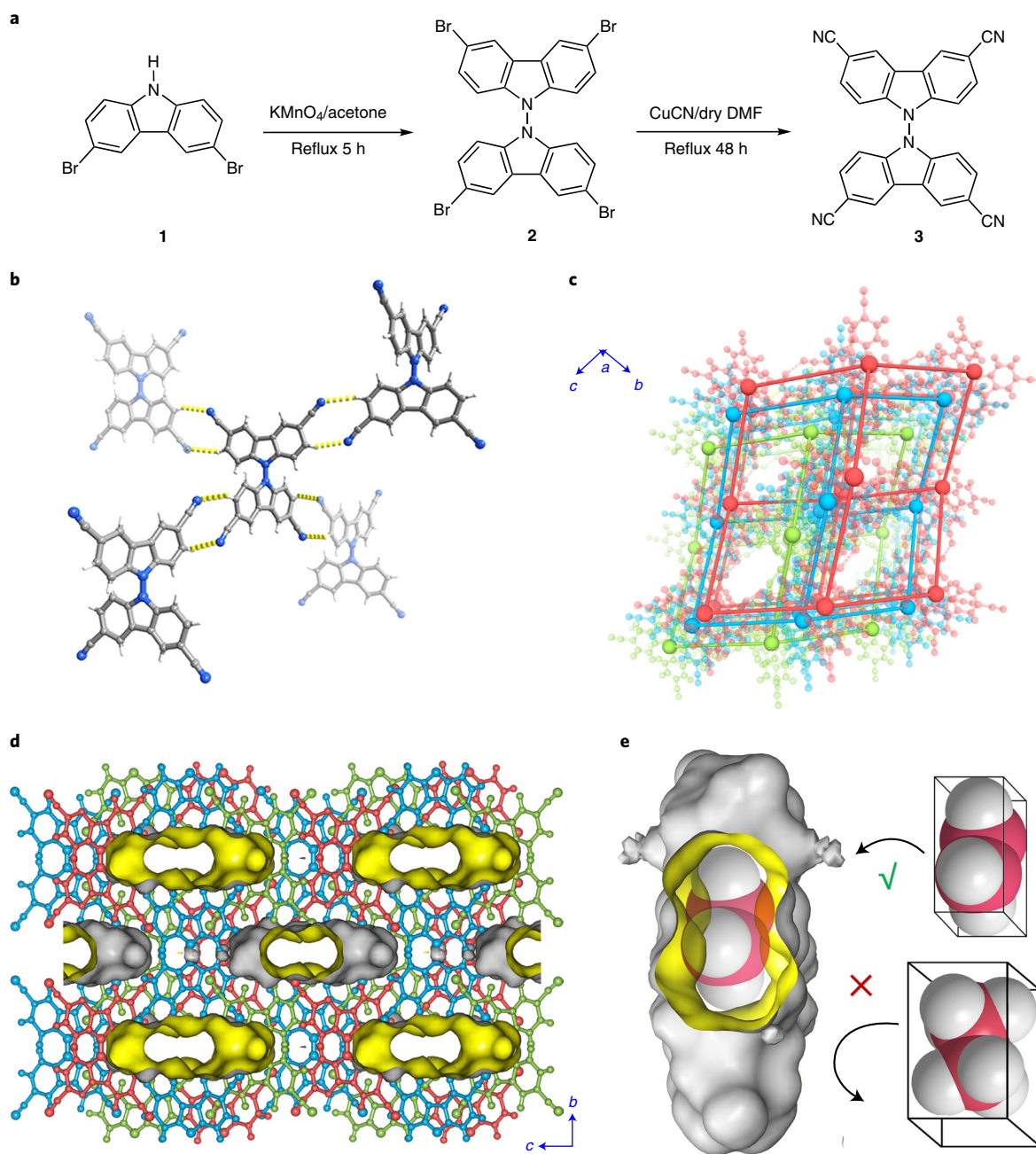


Fig. 2 | Crystal structure of HOF-FJU-1. **a**, A synthetic scheme of **3**, the organic building block for HOF-FJU-1. **b**, Adjacent building blocks—and, in turn, the extended network—are held together by intermolecular hydrogen bonding (yellow) involving the cyano groups. Grey, carbon; blue, nitrogen; white, hydrogen. **c**, The threefold-interpenetrated framework in dia topology; the three independent networks are shown in blue, red, and green, both in ball-and-stick representation and as a simplified structure (nods and rods). **d**, The framework (with the three interpenetrated networks shown in blue, red and green) with pore channels along the crystallographic [100] direction. **e**, A schematic diagram of the size-dependent separation for C_2H_4 and C_2H_6 molecules; the ethylene (top) and ethane (bottom) guest molecules are shown in sphere representation with carbon in red and hydrogen in white. In **d** and **e**, the pore surface is shown in yellow, framework surface in grey.

HOF-FJU-1a at 195 K and 1 bar (Supplementary Fig. 12). The stepwise adsorption isotherms for N_2 and CO_2 might indicate a flexible robust feature of HOF-FJU-1a (Supplementary Figs. 9 and 12). In situ PXRD patterns of HOF-FJU-1a following CO_2 loading at 195 K were collected to understand potential structural changes of the stepwise sorption behaviour. Only slight peak shift at (020) corresponding to minor expansion of pore window was identified during CO_2 loading (Supplementary Fig. 12), which indicates the flexibility of this HOF. We note that the stepwise adsorption behaviour

is accompanied by the flexibility of the HOF framework, in contrast to those from capillary condensation of mesopore in adsorbents with typical type-IV isotherms. On the other hand, there is no shifting on other diffraction peaks, which reveals certain robustness existing in HOF-FJU-1.

We further investigated the potential of HOF-FJU-1a for $\text{C}_2\text{H}_4/\text{C}_2\text{H}_6$ separation by collecting single-component adsorption isotherms for C_2H_4 and C_2H_6 at ambient conditions. At 298 K, the C_2H_4 sorption isotherm of HOF-FJU-1a showed a distinct sharp

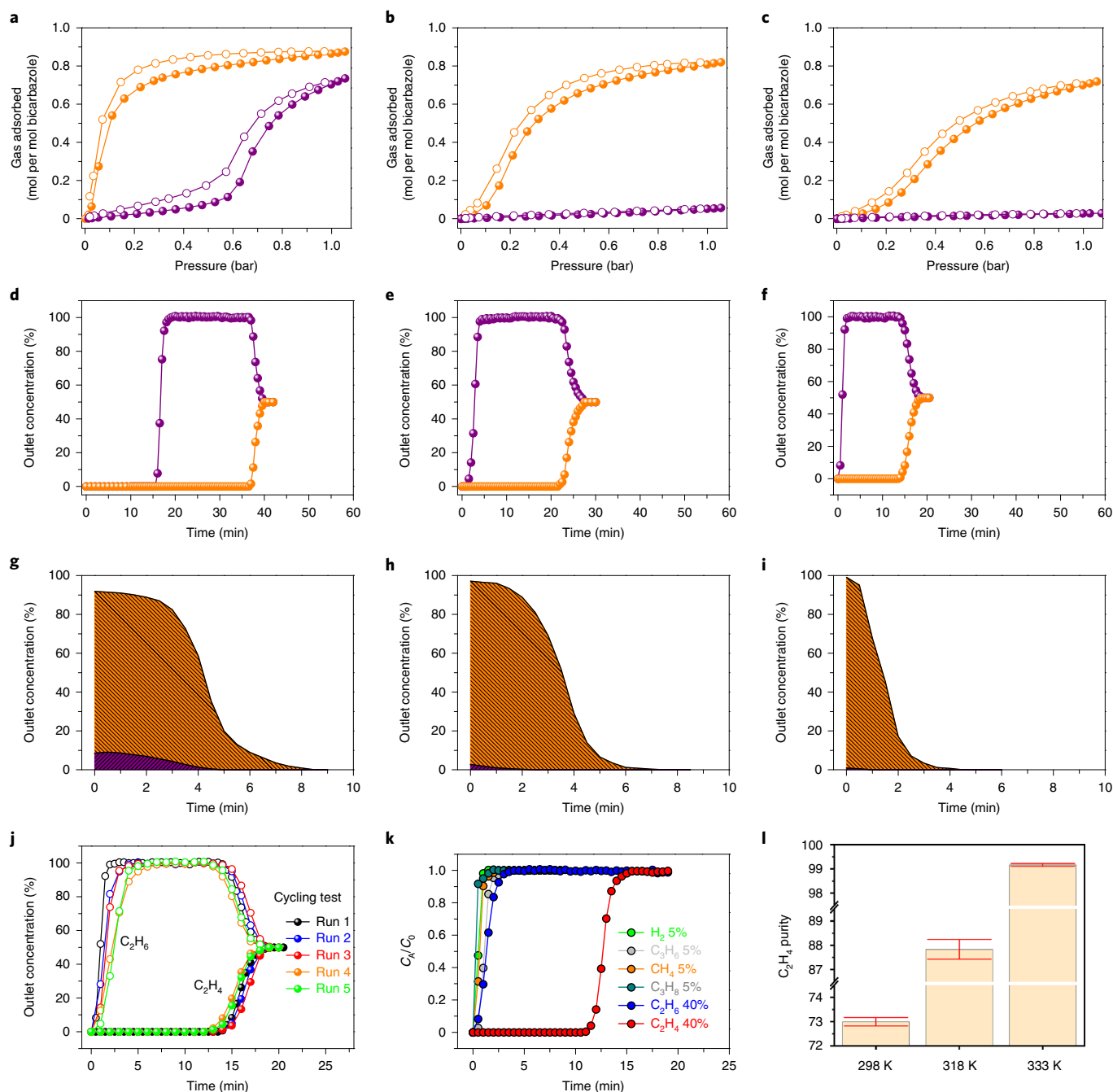


Fig. 3 | C_2H_4 and C_2H_6 sorption and separation in HOF-FJU-1a. **a–c**, Gas adsorption isotherms for ethylene and ethane in HOF-FJU-1a at 298 K (**a**), 318 K (**b**) and 333 K (**c**). Filled and open symbols represent adsorption and desorption, respectively. **d–f**, Breakthrough curves for C_2H_4/C_2H_6 mixture (50:50, v/v) in a fixed bed packed with HOF-FJU-1a at 298 K (**d**), 318 K (**e**) and 333 K (**f**). **g–i**, Concentration curves of the desorbed C_2H_4 from HOF-FJU-1a during the regeneration process. Desorption was carried out by applying vacuum at 298 K (**g**), 318 K (**h**) and 333 K (**i**). **j**, Multiple cycling tests of C_2H_4/C_2H_6 (50:50, v/v) mixtures. **k**, Breakthrough curves of HOF-FJU-1a for the $H_2/C_3H_6/CH_4/C_3H_8/C_2H_6/C_2H_4$ mixture (5:5:5:5:40:40, v/v/v/v/v/v) at 333 K and 1 bar. C_A and C_0 are the concentrations of each gas at the inlet and outlet, respectively. **l**, The purities of the C_2H_4 generated from HOF-FJU-1 during the regeneration processes of the fixed bed at different temperatures. The error bars denote \pm s.d. of the mean for $n=3$ independent experiments.

step at relatively low pressures (Fig. 3a), indicating that it was well accommodated in the compact pore space of this HOF and could undergo equilibrium adsorption even at low pressures and gas concentrations. The total C_2H_4 uptake at 1 bar and 298 K was $47 \text{ cm}^3 \text{ g}^{-1}$ (2.1 mmol g^{-1}). Surprisingly, HOF-FJU-1a showed negligible C_2H_6 uptake when the dosing pressure was below ~ 0.58 bar, followed by a steep rise after gate-opening with a total C_2H_6 uptake of $38 \text{ cm}^3 \text{ g}^{-1}$ at 1 bar.

These results indicate that HOF-FJU-1a showed high separation potential for C_2H_4/C_2H_6 at relatively low pressures. Given that the gate pressures will be increased at elevated temperatures, we further investigated the sorption behaviour of HOF-FJU-1a for C_2H_4 and C_2H_6 at 318 K and 333 K (Fig. 3b,c). Indeed, due to the increased gate-opening pressures at 333 K and 1 bar, HOF-FJU-1a shows a negligible uptake of $1 \text{ cm}^3 \text{ g}^{-1}$ (0.04 mmol g^{-1}) for C_2H_6 , which was lower than that of UTSA-280 (0.1 mmol g^{-1}) following sieve separation²⁹,

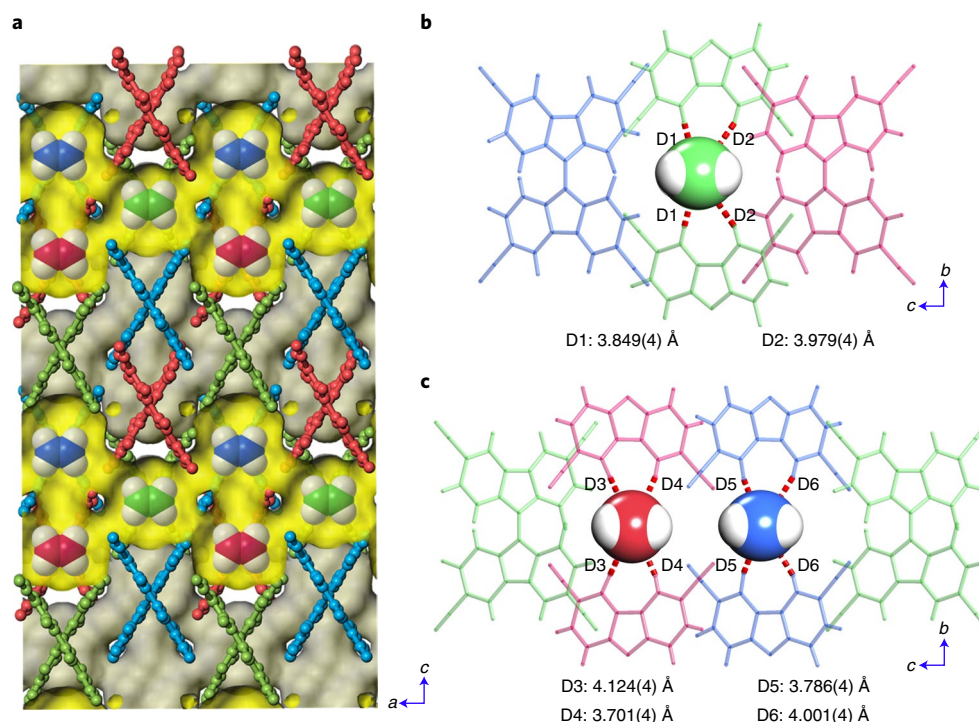


Fig. 4 | Single-crystal structure of HOF-FJU-1•0.94 C₂H₄. **a**, Top views of the packing diagram of the C₂H₄-loaded structure. The framework and pore surface are shown in grey and yellow. The HOF is shown in ball-and-stick representation; building blocks of each of the three interpenetrating networks are highlighted in blue, green and red, and the guests are shown in spherical representation. **b,c**, Preferential binding sites for C₂H₄ molecules and their close C-H... π (ethylene) contacts with the framework in the small neck (**b**) and in the large cage (**c**), respectively. The white spheres represent hydrogen atoms of C₂H₄, and the three crystallographically unique C₂H₄ molecules are shown with their respective carbon atoms in green, red and blue.

whereas steady C₂H₄ adsorption was still observed with a total uptake of 36 cm³ g⁻¹ (1.6 mmol g⁻¹). The loading-dependent isosteric heats of C₂H₄ adsorption in HOF-FJU-1a were calculated based on the adsorption isotherms at different temperatures to give a moderate value of 32 kJ mol⁻¹, which is consistent with physical adsorption^{17,42} (Supplementary Figs. 13 and 14). To further understand different adsorption behaviours for C₂H₄ and C₂H₆ in HOF-FJU-1a, in situ loading-dependent PXRD patterns of HOF-FJU-1a under atmosphere of C₂H₄ or C₂H₆ at related temperatures have been collected. As shown in Supplementary Figs. 15 and 16, at 298 K, both the C₂H₄- and C₂H₆-loading PXRD patterns show similar shifting of the (020) peaks, corresponding to slight structural transformation of pore window expansion. We note that the pressure where peak shifting started is consistent with corresponding gas sorption isotherms, which indicates the stepwise sorption is accompanied by expansion of pore window, referring to gate-opening. For C₂H₄-loading, similar gate-opening at higher pressure-threshold can be still observed at 318 K. By contrast, there is no noticeable structural transformation was observed for C₂H₆-loading indicated by corresponding PXRD patterns, consistent with negligible C₂H₆ uptake at 318 K. These results reveal that by applying different stimulus such as controlling the temperatures, flexible-robust HOFs can show corresponding response namely gate-opening to accommodate different gas molecules, thus realizing highly efficient separation.

Ideal adsorbed solution theory (IAST) calculations were then used to estimate the C₂H₄/C₂H₆ (50:50, v/v) separation selectivity at different temperatures. At 298 K, HOF-FJU-1a showed a moderate C₂H₄/C₂H₆ selectivity of 10.5 due to the co-adsorption of C₂H₆. After increasing the temperatures to 333 K where the co-adsorption of C₂H₆ was suppressed, the C₂H₄/C₂H₆ selectivity of HOF-FJU-1a increased to 42.3 at 1 bar (Supplementary Figs. 17–19, and Supplementary Tables 9 and 10), which was higher than those

of the benchmark UTSA-280 (15) and NOTT-300 (14.5) under the same operation conditions (Supplementary Figs. 20–22, and Supplementary Tables 11 and 12).

Although the high C₂H₄/C₂H₆ selectivity of HOF-FJU-1a is sufficient for high-purity ethylene capture, corresponding breakthrough tests in a fixed-bed column are prerequisite to validate the production purity of C₂H₄. We conducted fixed-bed breakthrough tests at 298 K to 333 K, in which the mixture of C₂H₄/C₂H₆ (50:50, v/v) was flowed over a packed column of activated HOF-FJU-1a sample, with a total flow of 1.25 ml min⁻¹ at different temperatures (Fig. 3d–f). At 298 K, although C₂H₄ capture was achieved, there was distinct C₂H₆ co-adsorption in the packed column of HOF-FJU-1a, as indicated by a moderate retention time for C₂H₆ in the breakthrough curves. Co-adsorption occurred due to the partial pressure of C₂H₆ in the gas mixture reached the borderline of gate-opening, and the production purity (the integration proportion of both concentration curves of desorbed C₂H₄ and C₂H₆ from the regeneration of HOF material) of C₂H₄ at 298 K was only 73.1 ± 0.1% (Fig. 3g).

In contrast, by tuning the gate-pressures to minimize co-adsorption of C₂H₆, the neat breakthrough curves of HOF-FJU-1a at 333 K showed an immediate C₂H₆ elution without any detectable C₂H₄, and very high C₂H₄ retention before the breakthrough of C₂H₄; thus, the C₂H₄ purity increased to 99.1 ± 0.1% at 333 K (Fig. 3h,i,l), which is higher than those performed by ITQ-55⁴³ and Cu(OPTz)³⁶, and almost identical to that of UTSA-280 (99.2%)²⁹. The captured C₂H₄ amount from the equimolar C₂H₄/C₂H₆ breakthrough curve at 333 K was calculated to be 0.407 mol kg⁻¹ (Supplementary Fig. 25), higher than those of UTSA-280 (0.326 mol kg⁻¹) and NOTT-300 (0.305 mol kg⁻¹) under the same conditions (Supplementary Figs. 23 and 24, and Supplementary Table 13). These results demonstrate that HOF-FJU-1a can realize high C₂H₄/C₂H₆ separation performance under mild conditions.

To evaluate durability, multiple cycling breakthrough experiments were performed under the same conditions, showing that HOF-FJU-1a can retain 97% of its captured C_2H_4 productivity after five cycles relative the first cycle (Fig. 3j and Supplementary Fig. 26). The effect of potential gas impurity in realistic conditions was also investigated. We performed a breakthrough study on a gas stream of $H_2/C_3H_6/CH_4/C_3H_8/C_2H_6/C_2H_4$ (5:5:5:5:40:40, v/v/v/v/v/v) and found that HOF-FJU-1a can still exclusively capture C_2H_4 from the mixture (Fig. 3k). Overall, these results demonstrate that high separation performance of C_2H_4 from relevant mixtures can be realized in HOF-FJU-1a.

We performed single-crystal X-ray diffraction measurements of C_2H_4 -loaded HOF-FJU-1a sample to determine the binding conformations of C_2H_4 . The data for HOF-FJU-1•0.94 C_2H_4 were collected at 100 K, from which the location of C_2H_4 molecules was identified by an increase in residual electron intensity (Supplementary Fig. 27 and Supplementary Table 1). Three crystallographically unique C_2H_4 molecules were identified in the compact pore channel (Fig. 4a). The C_2H_4 molecules were well dispersed along the one-dimensional pore channel with only host–guest interactions observed, showing multiple intermolecular interactions mainly C–H... π with the framework (3.701–4.124 Å) (Figs. 4b,c). A single-crystal X-ray diffraction study of HOF-FJU-1b (following ethane exposure) shows that there is no electron density in the open pore space (Supplementary Table 1), indicating that no ethane molecule was trapped. Modelling simulations indicate that—without taking into account the framework flexibility—the diffusion of both C_2H_4 and C_2H_6 molecules into HOF-FJU-1 is impossible (Supplementary Fig. 28). The substantial C_2H_4/C_2H_6 separation here might involve the dynamics of organic linkers.

Apart from the excellent C_2H_4/C_2H_6 separation performance, it is notable that (unusually for a HOF) HOF-FJU-1 exhibited excellent chemical stability, as validated by PXRD of samples following exposure to different harsh conditions. Although heating to 573 K led to framework decomposition, HOF-FJU-1 retained its crystallinity and porosity in aqueous solutions at pH values ranging from 1 to 14, and even in solutions of 12 M HCl and 10 M NaOH (Supplementary Figs. 29 and 30). Similarly, it was stable when immersed in various organic solvents including CH_2Cl_2 , hexane, 1,4-dioxane and acetonitrile, although not in N,N' -diethylformamide nor N,N' -dibutylformamide (Supplementary Figs. 30 and 31). The PXRD patterns showed peaks shift slightly as a result of the flexibility of the frameworks. Furthermore, HOF-FJU-1 was quickly regenerated from the N,N' -DMF (Supplementary Fig. 32). Many have reported that stable HOFs such as HOF-TCBP⁴⁴, PCF-1⁴⁵ and ZJU-HOF-1⁴⁶ are labile to basic solution and undergo deprotonation or hydrolysis. The strong intermolecular π - π stacking and hydrogen bonding interactions, compact structure for minor exposure of hydrogen-bonding motifs, and weak intrinsic acidity and basicity of cyano groups jointly endowed HOF-FJU-1 with excellent thermal and chemical stability in contrast to those HOFs with groups such as amides and carboxylic acids (Supplementary Table 2).

In summary, we have successfully realized a flexible robust hydrogen-bonded organic framework (HOF-FJU-1) with high sieving separation for ethylene from ethane by tuning the adsorption gate-pressures at different temperatures. This novel approach has successfully minimized the co-adsorption of ethane while retained a significant amount of ethylene uptakes, leading to considerably enhanced ethylene/ethane separation performance at the elevated temperatures. This HOF material can readily produce high-purity C_2H_4 (>99% pure) from C_2H_4/C_2H_6 mixture in a fixed-bed column at 333 K, a temperature close to the real gas mixture streams in practical processes, indicating the bright promise of this flexible-robust porous material for the industrial C_2H_4/C_2H_6 separation. Furthermore, HOF-FJU-1 is not only thermally stable but also stable in common organic solvents and pH values ranging from

1 to 14, even in solutions of 12 M HCl and 10 M NaOH. These results reveal the great application potentials of HOF-based materials for realizing important gas separations.

Online content

Any methods, additional references, Nature Research reporting summaries, source data, extended data, supplementary information, acknowledgements, peer review information; details of author contributions and competing interests; and statements of data and code availability are available at <https://doi.org/10.1038/s41557-021-00740-z>.

Received: 9 June 2020; Accepted: 28 May 2021;

Published online: 08 July 2021

References

- Sholl, D. S. & Lively, R. P. Seven chemical separations to change the world. *Nature* **532**, 435–437 (2016).
- Lin, J. Y. S. Molecular sieves for gas separation. *Science* **353**, 121–122 (2016).
- Chu, S., Cui, Y. & Liu, N. The path towards sustainable energy. *Nat. Mater.* **16**, 16–22 (2017).
- Kuznicki, S. M. et al. A titanosilicate molecular sieve with adjustable pores for size-selective adsorption of molecules. *Nature* **412**, 720–724 (2001).
- Kuznicki, S. M. & Bell, V. A. Olefin separations employing CTS molecular sieves. US Patent 6517611 (2003).
- Mohamed, M. H. et al. Designing open metal sites in metal–organic frameworks for paraffin/olefin separations. *J. Am. Chem. Soc.* **141**, 13003–13007 (2019).
- Furukawa, H., Cordova, K. E., O’Keeffe, M. & Yaghi, O. M. The chemistry and applications of metal–organic frameworks. *Science* **341**, 1230444 (2013).
- Li, L. et al. Ethane/ethylene separation in a metal–organic framework with iron-peroxo sites. *Science* **362**, 443–446 (2018).
- Liao, P.-Q., Zhang, W.-X., Zhang, J.-P. & Chen, X.-M. Efficient purification of ethene by an ethane-trapping metal–organic framework. *Nat. Commun.* **6**, 8697 (2015).
- Qazvini, T., Babarao, R., Shi, Z. L., Zhang, Y. B. & Telfer, S. G. A robust ethane-trapping metal–organic framework with a high capacity for ethylene purification. *J. Am. Chem. Soc.* **141**, 5014–5020 (2019).
- Yang, H. et al. Pore-space-partition-enabled exceptional ethane uptake and ethane-selective ethane–ethylene separation. *J. Am. Chem. Soc.* **142**, 2222–2227 (2020).
- Zeng, H. et al. Cage-interconnected metal–organic framework with tailored apertures for efficient C_2H_6/C_2H_4 separation under humid conditions. *J. Am. Chem. Soc.* **141**, 20390–20396 (2019).
- Hao, H.-G. et al. Simultaneous trapping of C_2H_2 and C_2H_6 from a ternary mixture of $C_2H_2/C_2H_4/C_2H_6$ in a robust metal–organic framework for the purification of C_2H_4 . *Angew. Chem. Int. Ed.* **130**, 16299–16303 (2018).
- Lin, L. et al. Fundamental insights into the reactivity and utilization of open metal sites in Cu (I)-MFU-4l. *Organometallics* **38**, 3453–3459 (2019).
- Wang, H. et al. One-of-a-kind: a microporous metal–organic framework capable of adsorptive separation of linear, mono- and di-branched alkane isomers via temperature- and adsorbate-dependent molecular sieving. *Energy Environ. Sci.* **11**, 1226 (2018). Based on the 77 K N_2 isotherms, flexible-robust phenomena have not been clearly observed in this calcium MOF.
- Huang, N., Wang, P. & Jiang, D. Covalent organic frameworks: a materials platform for structural and functional designs. *Nat. Rev. Mater.* **1**, 16068 (2016).
- Li, B. et al. Introduction of π -complexation into porous aromatic framework for highly selective adsorption of ethylene over ethane. *J. Am. Chem. Soc.* **136**, 8654–8660 (2014).
- He, Y., Xiang, S. & Chen, B. A microporous hydrogen-bonded organic framework for highly selective C_2H_2/C_2H_4 separation at ambient temperature. *J. Am. Chem. Soc.* **133**, 14570–14573 (2011).
- Lin, R.-B. et al. Multifunctional porous hydrogen-bonded organic framework materials. *Chem. Soc. Rev.* **48**, 1362–1389 (2019).
- Liao, P.-Q., Huang, N.-Y., Zhang, W.-X., Zhang, J.-P. & Chen, X.-M. Controlling guest conformation for efficient purification of butadiene. *Science* **356**, 1193–1196 (2017).
- Chen, K.-J. et al. Synergistic sorbent separation for one-step ethylene purification from a four-component mixture. *Science* **366**, 241 (2019).
- Zhang, X. et al. Selective ethane/ethylene separation in a robust microporous hydrogen-bonded organic framework. *J. Am. Chem. Soc.* **142**, 633–640 (2020).
- Vaidhyanathan, R. et al. Direct observation and quantification of CO_2 binding within an amine-functionalized nanoporous solid. *Science* **330**, 650–653 (2010).

24. Bloch, E. D. et al. Hydrocarbon separations in a metal–organic framework with open iron(II) coordination sites. *Science* **335**, 1606–1610 (2012).
25. Yang, S. et al. Supramolecular binding and separation of hydrocarbons within a functionalized porous metal–organic framework. *Nat. Chem.* **7**, 121–129 (2014).
26. Cui, X. et al. Pore chemistry and size control in hybrid porous materials for acetylene capture from ethylene. *Science* **353**, 141–144 (2016).
27. Yoon, J. W. et al. Selective nitrogen capture by porous hybrid materials containing accessible transition metal ion sites. *Nat. Mater.* **16**, 526–531 (2016).
28. Wang, H. et al. Tailor-made microporous metal–organic frameworks for the full separation of propane from propylene through selective size exclusion. *Adv. Mater.* **30**, 1805088 (2018).
29. Lin, R.-B. et al. Molecular sieving of ethylene from ethane using a rigid metal–organic framework. *Nat. Mater.* **17**, 1128–1133 (2018).
30. Cadiou, A., Adil, K., Bhatt, P. M., Belmabkhout, Y. & Eddaoudi, M. A metal–organic framework-based splitter for separating propylene from propane. *Science* **353**, 137–140 (2016).
31. Bavykina, A. & Gascon, J. An efficient nanosieve. *Nat. Mater.* **17**, 1057–1058 (2018).
32. Reid, C. R. & Thomas, K. M. Adsorption kinetics and size exclusion properties of probe molecules for the selective porosity in a carbon molecular sieve used for air separation. *J. Phys. Chem. B* **105**, 10619–10629 (2001).
33. Webster, C. E., Drago, R. S. & Zerner, M. C. Molecular dimensions for adsorptives. *J. Am. Chem. Soc.* **120**, 5509–5516 (1998).
34. Li, L. et al. A metal–organic framework with suitable pore size and specific functional sites for the removal of trace propyne from propylene. *Angew. Chem. Int. Ed.* **57**, 15183–15188 (2018).
35. Krause, S. et al. A pressure-amplifying framework material with negative gas adsorption transitions. *Nature* **532**, 348–352 (2016).
36. Gu, C. et al. Design and control of gas diffusion process in a nanoporous soft crystal. *Science* **363**, 387 (2019).
37. Yang, H. et al. Lock-and-key and shape-memory effects in an unconventional synthetic path to magnesium metal–organic frameworks. *Angew. Chem. Int. Ed.* **58**, 11757–11762 (2019).
38. Kitaura, R., Seki, K., Akiyama, G. & Kitagawa, S. Porous coordination-polymer crystals with gated channels specific for supercritical gases. *Angew. Chem. Int. Ed.* **42**, 428–431 (2003).
39. Li, L. et al. Flexible-robust metal–organic framework for efficient removal of propyne from propylene. *J. Am. Chem. Soc.* **139**, 7733–7736 (2017). “Flexible-robust MOF” has been defined for the first time in this literature, as shown in Fig. 1b. The “flexible-robust” has been also clarified in illustration on the N₂ and CO₂ adsorption of HOF-FJU-1a (Supplementary Figs. 9 and 12) at cryogenic temperatures.
40. Sarkisov, L. & Harrison, A. Computational structure characterisation tools in application to ordered and disordered porous materials. *Mol. Simul.* **37**, 1248–1257 (2011).
41. Thommes, M. et al. Physisorption of gases, with special reference to the evaluation of surface area and pore size distribution. *Pure Appl. Chem.* **87**, 1051–1069 (2015).
42. Aguado, S., Bergeret, G., Daniel, C. & Farrusseng, D. Absolute molecular sieve separation of ethylene/ethane mixtures with silver zeolite A. *J. Am. Chem. Soc.* **134**, 14635–14637 (2012).
43. Bereciartua, P. J. et al. Control of zeolite framework flexibility and pore topology for separation of ethane and ethylene. *Science* **358**, 1068–1071 (2017).
44. Hu, F. L. et al. An ultrastable and easily regenerated hydrogen-bonded organic molecular framework with permanent porosity. *Angew. Chem. Int. Ed.* **56**, 2101–2104 (2017).
45. Yin, Q. et al. An ultra-robust and crystalline redeemable hydrogen-bonded organic framework for synergistic chemo-photodynamic therapy. *Angew. Chem. Int. Ed.* **57**, 7691–7696 (2018).
46. Zhang, X. et al. A rod-packing hydrogen-bonded organic framework with suitable pore confinement for benchmark ethane/ethylene separation. *Angew. Chem. Int. Ed.* **60**, 10304–10310 (2021).

Publisher's note Springer Nature remains neutral with regard to jurisdictional claims in published maps and institutional affiliations.

© The Author(s), under exclusive licence to Springer Nature Limited 2021

Methods

Materials. 3,6-Dibromocarbazole (99%, HWG), potassium permanganate (99.5%, SCRC), acetone (99.5%, SCRC), cuprous cyanide (99.5%, SCRC), anhydrous ferric chloride (98%, Sigma-Aldrich) and anhydrous DMF (99%, Sigma-Aldrich) were purchased and used without further purification. N₂ (99.999%), C₂H₄ (99.99%), C₂H₆ (99.99%), He (99.999%), C₂H₄/C₂H₆ = 50/50 (v/v) and H₂/C₂H₄/CH₄/C₂H₆/C₂H₂/C₂H₄ (5/5/5/5/40/40, v/v/v/v/v) were purchased from Beijing Special Gas (China).

Synthesis of 3,3',6,6'-tetrabromo-9,9'-bicarbazole (2). Potassium permanganate (2.371 g, 15 mmol) was added at 323 K to a solution of 3,6-dibromocarbazole (1) (1.625 g, 5 mmol) in 25 ml acetone and then the solution was stirred for 5 h at 333 K with a reflux condenser and cooled to room temperature. After removal of the organic solvents, the residue was extracted with CHCl₃ (250 ml) for 12 h with stirring. The filtrate was washed three times with CHCl₃. The residue was purified by recrystallization from chloroform/hexane to give colourless crystals (0.83 g, 51% yield). ¹H NMR (400 MHz, DMSO-*d*₆): δ = 8.72 (d, 4 H, *J* = 1.9 Hz), 7.55 (dd, 4 H, *J* = 8.6, 1.9 Hz), 6.91 (d, 4 H, *J* = 8.7 Hz).

Synthesis of 3,3',6,6'-tetracyano-9,9'-bicarbazole (3). A mixture of CuCN (2.782 g, 31.06 mmol) and compound 2 (2 g, 3.086 mmol) in dry DMF (50 ml) was added to a 120 ml Schleck flask charge with stir bar and reacted at 423 K for 48 h under N₂ atmosphere. After cooling to room temperature, concentrated HCl (40 ml) and iron(III) trichloride (30 g, 184.9 mmol) were added to the mixture and stirred under 273 K for 2 h. The reaction mixture was diluted with water (200 ml), filtered and the grey coloured solid was collected (1.3 g, 97% yield); melting point = 574.5 K. ¹H NMR (400 MHz, DMSO-*d*₆): δ 9.10 (s, 4 H), 7.91 (d, 4 H, *J* = 8.5 Hz), 7.32 (d, 4 H, *J* = 8.7 Hz); ¹³C NMR (400 MHz, DMSO-*d*₆) δ = 141.45, 131.69, 127.12, 121.38, 119.22, 110.51, 105.12; IR (KBr): 2,225 (ν_{CN}), 1,602, 1,485, 1,451, 1,365, 1,292, 1,238, 1,186, 1,137, 1,028, 893, 815, 587 cm⁻¹. The compound was best formulated as HOF-FJU-1·DMF·10H₂O. TGA data: calculated weight loss for 1 DMF and 10 H₂O molecules: 33.44%; found: 35.60%; calculated elemental analysis (found for C₄₈H₃₂N₁₁O₁₂): C (59.13%, 59.31%), H (5.37%, 5.34%), N (15.80%, 15.82%).

Crystallization of the organic building block (HOF-FJU-1). The organic building block (3) (0.1 g, 0.23 mmol) was dissolved in DMF (2 ml) under 403 K in a glass flask. The resulting solution was cooled to room temperature (296 K) for 12 h. Colourless needle-like crystals were obtained. The PXRD results showed that the synthesized HOF-FJU-1 is a pure phase (Supplementary Fig. 1).

Sample characterization. The crystallinity and phase purity of the samples were measured using PXRD with a Rigaku Ultima IV X-ray diffractometer with copper Kα radiation (λ = 1.54184 Å), under N₂ atmosphere, scanning over the 5° to 30° range. The Fourier-transform infrared (KBr pellets) spectra were recorded in the 400–4,000 cm⁻¹ range on Thermo Nicolet 5700 FT-IR instruments. ¹H NMR and ¹³C NMR experiments were performed on Bruker Advance III 400 MHz. Thermogravimetric analyses were performed with METTLER Q50 under N₂ atmosphere with a heating rate of 10 K min⁻¹ from 313 K to 973 K. A micromeritics ASAP 2020 HD surface area analyser was used to measure gas adsorption isotherms. Guest-free HOF-FJU-1 (0.120 g) was made from fresh sample (0.133 g), vacuumed at room temperature for 24 h and further at 423 K until the outgas rate was 5 mm Hg min⁻¹ before measurements. The N₂ adsorption was tested at 77 K using liquid nitrogen to maintain the temperature, ethane and ethylene were tested at 273 K, 298 K, 318 K and 333 K, respectively. The single-crystal X-ray was performed with Agilent Technologies SuperNova A diffractometer and the structures were solved by direct methods and refined by full matrix least-squares methods with the SHELXT program package. The pore size of HOF-FJU-1 was calculated by Poreblazer⁴⁷ program on the basis of the crystal structure. The probe in the application to the pore size distribution calculations was a nitrogen atom 3.31 Å in collision diameter. Elemental analyses were performed on a Vario EL III analyser.

Single-crystal X-ray diffraction studies. Data collection and structural analysis of the crystals were collected on an Agilent Technologies SuperNova single-crystal diffractometer equipped with graphite monochromatic copper Kα radiation (λ = 1.54184 Å). Using Olex2, the structure was solved with the ShelXT structure solution program using intrinsic phasing and refined with the SHELXT refinement package using least-squares minimization⁴⁸.

The HOF-FJU-1 single crystal was kept at 293 K during data collection. The highest peak (1.68 eÅ⁻³) in the structure of HOF-FJU-1 was located 2.70 Å from a hydrogen atom in bicarbazole. The solvent molecules in HOF-FJU-1 were highly disordered and no satisfactory disorder model could be accomplished. A region of solvent electron density was thus treated with the SQUEEZE program in PLATON. After squeeze, the highest peak (0.26 eÅ⁻³) in the structure of HOF-FJU-1 was located 0.23 Å from a hydrogen atom in bicarbazole. All non-hydrogen atoms were refined with anisotropic displacement parameters. The hydrogen atoms on the framework were placed in idealized positions and refined using a riding model.

The single crystal of HOF-FJU-1 was fixed inside of a glass capillary and pretreated in a manner similar to the gas adsorption measurement to obtain guest-free HOF-FJU-1a. After the single-crystal data collection for guest-free HOF-FJU-1a in N₂ atmosphere, the capillary with one open end was placed in a desiccator to backfill with C₂H₄ or C₂H₆ for 12 h to get the gas loaded single crystal. The desiccator was filled with C₂H₄ or C₂H₆ through ASAP 2020 HD, and the pressure inside of the desiccator was measured to be 1 atm. The capillary was then sealed with plasticine and kept at 100 K during data collection for HOF-FJU-1a or HOF-FJU-1b. The non-hydrogen atoms were refined anisotropically and the non-hydrogen atoms, except for C₂H₄ molecules, were fixed at calculated positions. The hydrogen atoms of the C₂H₄ molecules were added and refined by using a riding model. The restraints (DFIX) were used for the C₂H₄ molecules (C–C distance). The occupancy of the guest C₂H₄ molecule was refined by introducing partial occupancy. For the C₂H₄ molecules, the carbon atoms were refined at a fixed occupancy factor of 0.76, 0.59 and 0.52 for C43, C44 and C45, respectively. Both checkCIF results of HOF-FJU-1a and HOF-FJU-1b indicate there is one A-level alert in each structure regarding solvent accessible voids. For HOF-FJU-1a, the solvent accessible voids (270 Å³ per unit cells) can be attributed to the removal of solvent molecules on heating before data collection. For HOF-FJU-1b, the solvent-accessible voids (253 Å³ per unit cells) occur as there are not any guest molecules that can be recognized from the very weak residual electron density peaks during crystallographic refinement.

In-situ gas-loaded PXRD. In situ gas-loaded PXRD patterns were recorded by using a PANalytical X'Pert³ powder diffractometer equipped with a copper sealed tube (λ = 1.54056 Å) at 40 kV and 40 mA. An Anton Paar TTK 600 stage coupled with an Anton Paar CCU 100 Temperature Control Unit was used to control the temperature. In a typical experiment, 20 mg of sample was activated and loaded on a zero-background sample holder made for an Anton Paar TTK 600 chamber. The data were collected from 5° to 30° (2θ) with a step-size of 0.0131303° and a scan time of 40 s per step. The sample was cooled from the room temperature to 195 K by using liquid nitrogen set up for Anton Paar TTK 600. Once the chamber and the sample were cooled to 195 K, then CO₂ was dosed in the chamber under different pressures corresponding to the CO₂ adsorption isotherm. Ethylene and ethane were tested in the same way at 298 K and 318 K. The PXRD patterns are recorded after equilibration (30 min) at selected points of the isotherm, as show in Supplementary Figs. 12, 15 and 16.

The isosteric enthalpies of adsorption. The isosteric enthalpy of adsorption for C₂H₄ and C₂H₆ were calculated using the data collected at 318 K and 333 K. The data were fitted using a virial-type expression composed of parameters *a*_{*i*} and *b*_{*i*} (Equation (1)),

$$\ln p = \ln N + \frac{1}{T} \sum_{i=0}^m a_i N_i + \sum_{i=0}^n b_i N_i \quad (1)$$

where *p* is the pressure (mm Hg), *T* is the temperature (kelvin), *R* is the universal gas constant (8.314 J mol⁻¹ K⁻¹), *N* is the amount adsorbed (mg g⁻¹), and *m* and *n* determine the number of terms required to adequately describe the isotherm. The isosteric enthalpies of adsorption *Q*_{st} (kJ mol⁻¹) were then calculated from the fitting parameters using (Equation (2)), only data point at zero or near-zero coverage is claimed to illustrate the adsorption enthalpy:

$$Q_{st} = -R \sum_{i=0}^m a_i N_i \quad (2)$$

Prediction of the gas adsorption selectivity by IAST. Fitting details: the adsorption data for C₂H₄ and C₂H₆ in HOF-FJU-1 at 273, 298, 318 and 333 K were fitted with single-site Langmuir-Freundlich equation.

$$N = N^{\max} N \frac{bp^{1/n}}{1 + bp^{1/n}} \quad (3)$$

where *p* is the pressure of the bulk gas in equilibrium with the adsorbed phase (kPa), *N* is the amount adsorbed per mass of adsorbent (mmol g⁻¹), *N*^{max} is the saturation capacities of site 1 (mmol g⁻¹), *b* is the affinity coefficient of site 1 (1/kPa) and *n* represents the deviations from an ideal homogeneous surface; the corresponding isotherm fit parameters for C₂H₄ and C₂H₆ in UTSA-280 and NOTT-300 at 318 and 333 K are provided in Supplementary Figs. 20 and 21.

IAST calculation: the adsorption selectivity based on IAST for mixed C₂H₄/C₂H₆ is defined by the following equation:

$$S_{A/B} = \frac{q_A y_B}{q_B y_A} \quad (4)$$

where *q*_{*i*} and *y*_{*i*} are the mole fractions of component *i* (*i* = A, B) in the adsorbed and bulk phases, respectively.

Breakthrough experiments. The breakthrough experiments for C₂H₄/C₂H₆ (50:50, v/v) gas mixtures were carried out at a flow rate of 1.25 ml min⁻¹. Activated HOF-FJU-1a (1.10 g), UTSA-280 (1.17 g) and NOTT-300 (1.12 g)

powder were packed into ϕ 3 × 300 mm stainless steel column. The experimental set-up consisted of two fixed-bed stainless steel reactors. One column was loaded with the adsorbent and kept at different temperatures (298 K, 318 K and 333 K), whereas the other reactor was used as a blank control group to stabilize the gas flow. The flow rates of all gas mixtures were regulated by mass flow controllers, and the effluent gas stream from the column is monitored by a gas chromatography (Thermal Conductivity Detector, detection limit 0.1%). Before the breakthrough experiment, we flushed the activated sample in adsorption bed with helium gas (100 ml min⁻¹) for 30 min at 333 K to ensure the total removal of adsorbed gas. The production purity is calculated based on the integration proportion of both concentration curves of desorbed C₂H₄ and C₂H₆ from the regeneration of HOF material. By contrast, as C₂H₆-selective adsorbents can directly produce pure C₂H₄ in one single separation step, their recovered purity of ethylene is calculated based on the concentration ratio of C₂H₄ and C₂H₆ in the outlets of the column.

Data availability

All data supporting the finding of this study are available within this article and its Supplementary Information. Crystallographic data for the structures in this article have been deposited at the Cambridge Crystallographic Data Centre under deposition nos. CCDC 1878390 (HOF-FJU-1), 1871845 (HOF-FJU-1⊃H₂O), 1999088 (HOF-FJU-1a), 1942488 (HOF-FJU-1⊃C₂H₄) and 1999090 (HOF-FJU-1b). Copies of the data can be obtained free of charge from <https://www.ccdc.cam.ac.uk/structures/>. Source data are provided with this paper.

References

47. Sarkisov, L. & Harrison, A. Computational structure characterisation tools in application to ordered and disordered porous materials. *Mol. Simul.* **37**, 1248–1257 (2011).
48. Sheldrick, G. M. SHELXT-Integrated space-group and crystal-structure determination. *Acta Crystallogr. A* **71**, 3–8 (2015).

Acknowledgements

We gratefully acknowledge the financial support from the National Natural Science Foundation of China (grant nos. 21975044, 21971038 and 21922810), the Fujian Provincial Department of Science and Technology (grant nos. 2019H6012 and 21019L3004) and the Welch Foundation (grant no. AX-1730).

Author contributions

Y.S.Y., L.L., R.-B.L., Z.J.Z., S.C.X. and B.L.C. conceived the research idea and designed the experiments. Y.S.Y. performed most of the experiments and analysed the data. L.L. and L.Y. measured the laboratory-scale fixed-bed breakthrough tests of HOF-FJU-1. Y.S.Y., L.L., R.-B.L., Z.J.Z., S.C.X. and B.L.C. wrote the paper. All authors discussed the results and commented on the manuscript. Y.S.Y., L.L. and R.-B.L. contributed equally to this work.

Competing interests

The authors declare no competing interests.

Additional information

Supplementary information The online version contains supplementary material available at <https://doi.org/10.1038/s41557-021-00740-z>.

Correspondence and requests for materials should be addressed to Z.Z., S.X. or B.C.

Peer review information *Nature Chemistry* thanks Ashleigh Fletcher, Ichiro Hisaki, Claire Hobday and the other, anonymous, reviewer(s) for their contribution to the peer review of this work.

Reprints and permissions information is available at www.nature.com/reprints.